Lecture 27
Other Emerging dAFM Techniques

Arvind Raman

Mechanical Engineering
Birck Nanotechnology Center

Other emerging dAFM techniques

- High-speed/video rate AFM
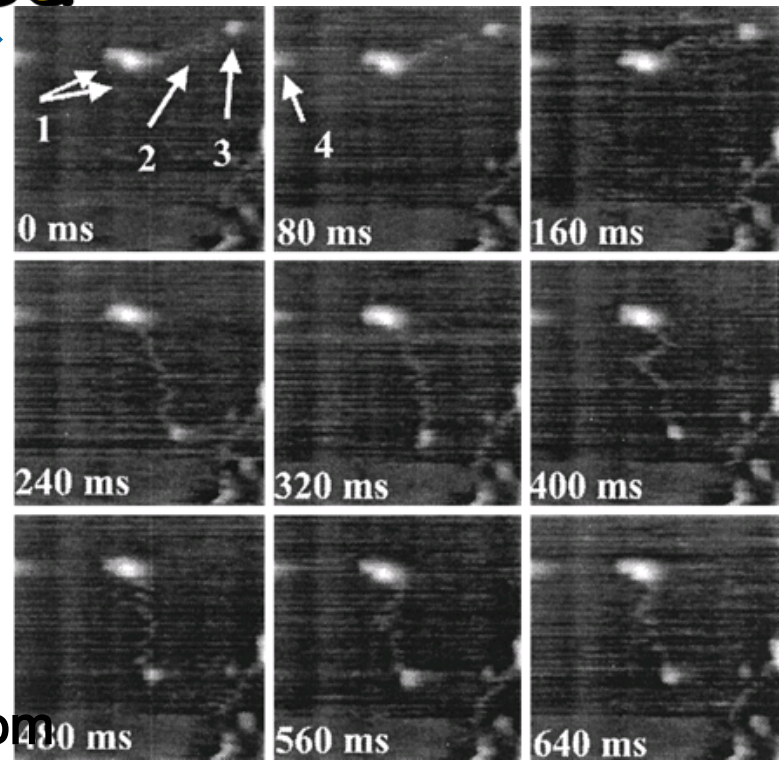- Multi-frequency AFM
- Sub-surface imaging

The driving forces

- Primary needs
  - High speed
  - High resolution
  - Material contrast – mechanical, electrical, chemical, thermal to distinguish a variety of samples
  - Quantitative metrology

- Newer needs
  - Subsurface information
  - Live cell imaging
 - Combined instruments (Raman, IR/thermal etc.)

High speed AM-AFM in liquids →

T. Ando et al, 2001, PNAS, Successive images of myosin V on mica in buffer solution. 240 × 240 nm² was imaged 50 times with 100 × 100 pixels. The tip speed is 0.6 mm/s (scan rate, 1.25 kHz), and the frame rate is 12.5/s. The tapping frequency is 620 kHz, A_0=12 nm, A=11.5 nm.
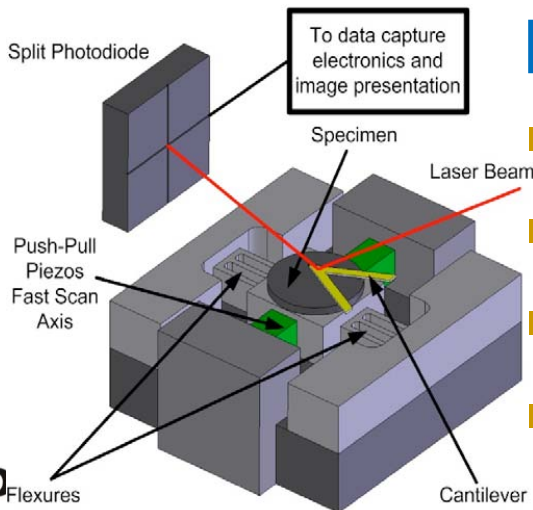
- M. Miles et al.
- T. Fukuma et al
- G. Schitter et al
- G. Fantner et al.
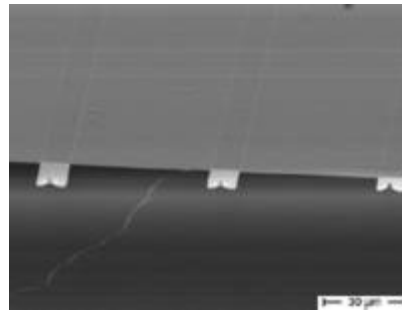
www.sclsensortech.com

Enabling technologies

- High bandwidth Scanner, Z piezo,
- Fast phase detection
- Small cantilevers (< 20 microns)
- Excitation mechanisms (photothermal, high bandwidth magnetic)

Split Photodiode

To data capture electronics and image presentation

Specimen

Laser Beam

Push-Pull Piezos Fast Scan Axis

Cantilever

P Flexures

UNIVERSITY

4

High-speed AFM

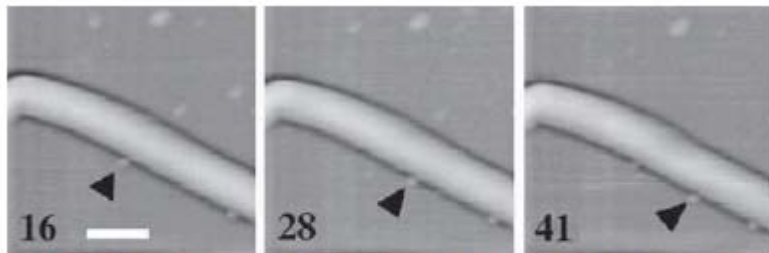T. Ando et al, Kanazawa (Pflugers Archiv, 2008)

Fig. 3 Movement of kinesin–gelsolin along a microtubule. The number attached to each image indicates the time (s) elapsed after imaging began. The arrowheads point at kinesin–gelsolin. *Scale bar*, 100 nm; imaging rate, 0.64 s/frame

M . J. Miles, Bristol, (APL, 86, 2005)

- Infinitesima Inc.

Fig. 7 Three-dimensional images of actin filament sliding movement captured by high-speed AFM. The number attached to each image indicates the time (s) elapsed after imaging began. *Scale bar* 30 nm, imaging rate, 180 ms/frame

split photo-diode
Direct force applied to end of probe
Laser
External force applied to cantilever base
Sample mounted on tuning fork.
Cantilever
Piezo for slow scan axis (~30Hz)
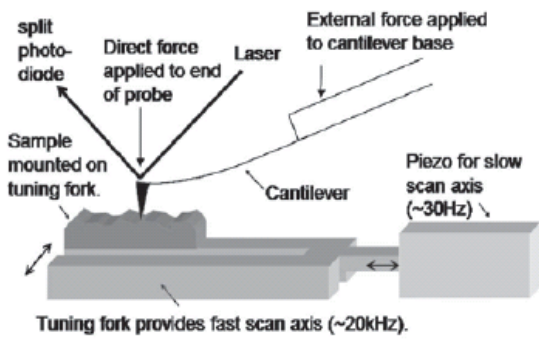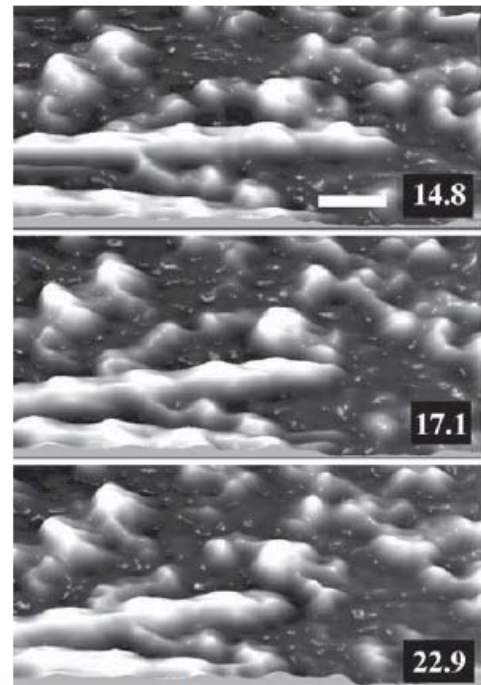Tuning fork provides fast scan axis (~20kHz).

FIG. 1. A schematic of the HSAFM. The sample is mounted on a quartz crystal resonator that generates the fast scan axis and is driven in the orthogonal slow scan axis by a piezo actuator. An optical lever is used to measure the deflection of the microcantilever. An additional "direct force" is applied to the end of the cantilever, forcing the tip to maintain contact with the surface. By tuning the magnitude of the "direct force" and the degree of damping of the cantilever, a high bandwidth passive feedback loop is created.
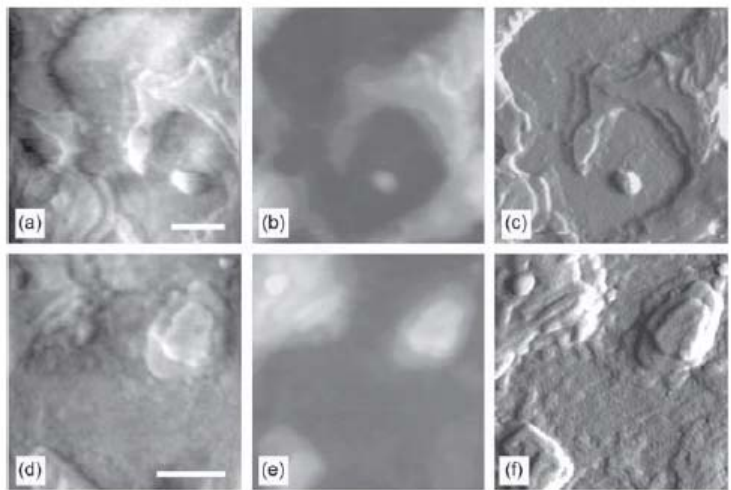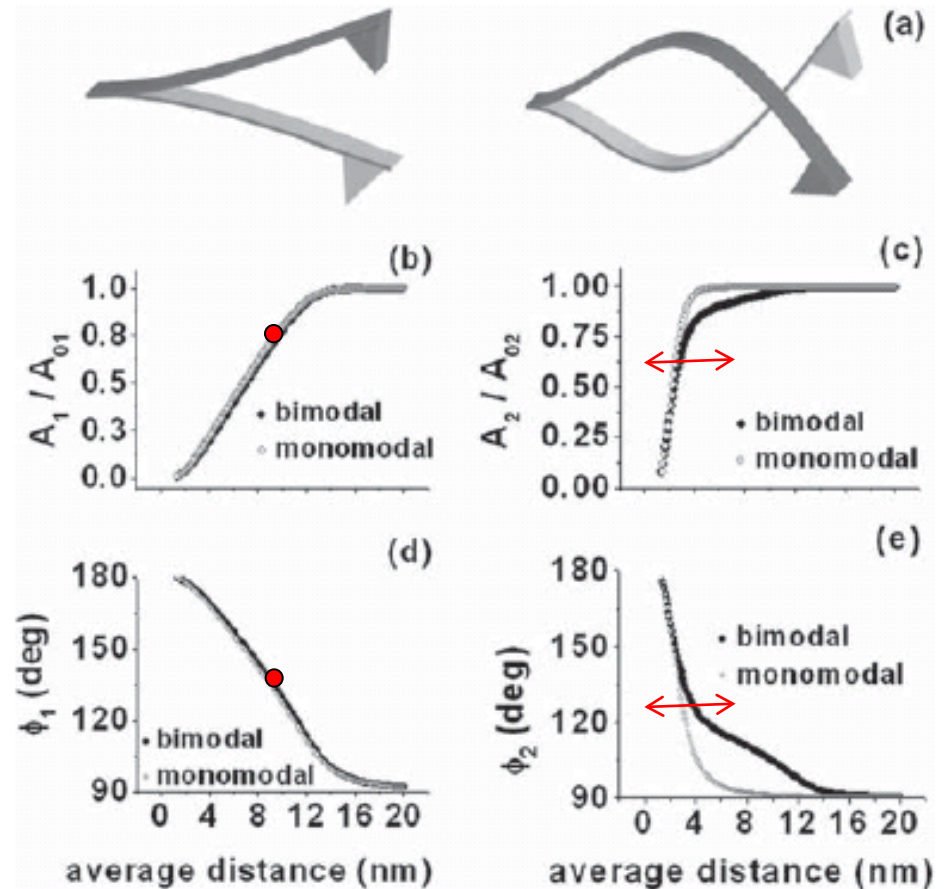
FIG. 2. The images show the surface of crystallized poly(ethylene-oxide) (PEO) on a glass substrate collected using both conventional AFM and HSAFM. (a) and (d) were collected using HSAFM over a period of 14.3 and 15.8 ms with a tip velocity in the centre of the image of 22.4 and 16.8 cm/s, respectively (128 × 128 pixels). (b) and (c) show the same area of the sample as image (a) and were collected using conventional AFM displaying the height and deflection of the cantilever (error signal), respectively. (e) and (f) show the same area of the sample as image (d) and were collected using conventional AFM displaying the height and deflection of the cantilever (error signal), respectively. The surface of the soft polymer sample showed no degradation after repeated imaging using both conventional and high speed AFM. Scales bars are 1 μm. Black to white in (b) represents 200 nm, and in (c) represents 180 nm. The information in the HSAFM images are a combination of topographic height and slope information, so the z scale does not have a defined unit or calibration.

Multi-frequency AFM

- Bimodal or dual AC
  - Key insight is that the second mode A_2, ϕ_2 varies in time
  - Thus ϕ_2 not only measures dissipation but also conservative tip-sample interactions!
  - It becomes possible to see material contrast in the attractive regime!

(a)

(b) A_1 / A_{01} — bimodal, monomodal

(c) A_2 / A_{02} — bimodal, monomodal

(d) ϕ_1 (deg) — bimodal, monomodal

(e) ϕ_2 (deg) — bimodal, monomodal

average distance (nm)

Rodriguez and Garcia, APL,84(3), 2004
Lozano and Garcia, PRL, 100(7), 2008
Lozano, Garcia, PRB, 79(1), 2009
R. Proksch, APL, 89(11), 2006

PURDUE
UNIVERSITY

6

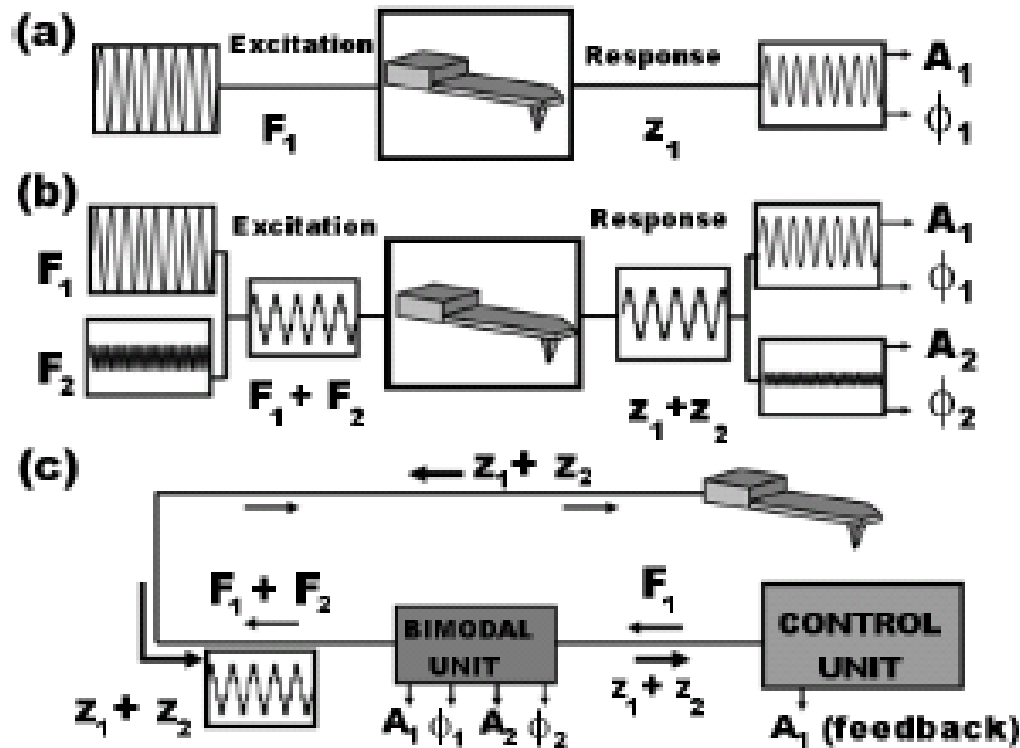# Multi-frequency AFM

- Bimodal or dual AC

Figure 1. Comparison between amplitude modulation and bimodal AFM. (a) AM-AFM (monomodal excitation). (b) Bimodal AFM. (c) Schematics of the bimodal AFM instrument. The bimodal excitation/detection unit performs the multifrequency excitation and the multicomponent signal processing while the control unit runs the feedback.

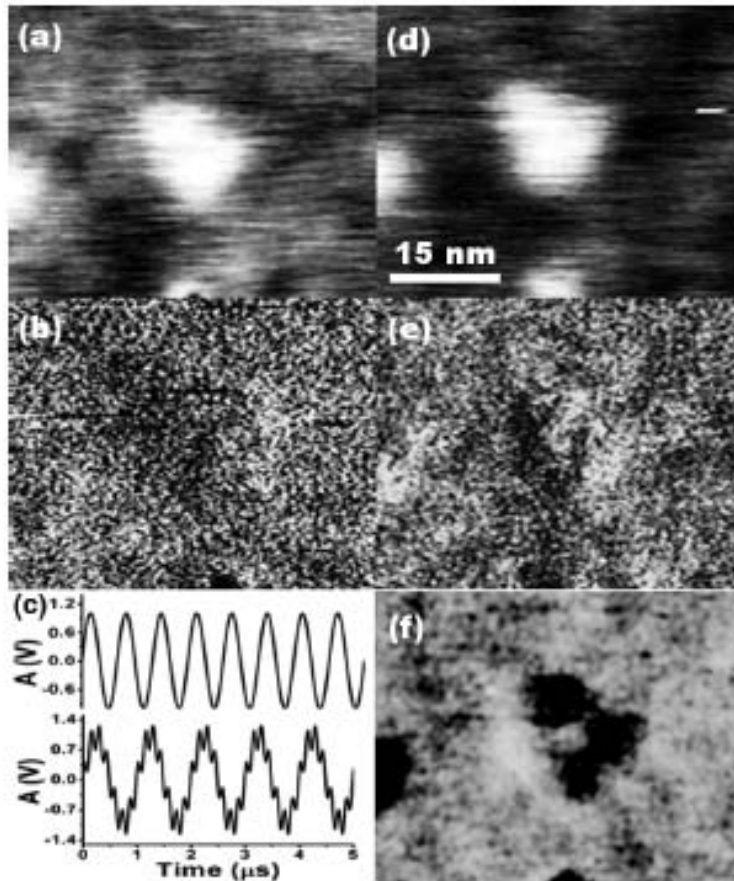# Multi-frequency AFM

■ Bimodal or dual AC

Figure 3. Comparison between AM-AFM and bimodal AFM images of IgG antibodies. (a) Topography and (b) phase images of an IgG obtained in AM-AFM. (c) Tip oscillation in AM-AFM (top) and bimodal AFM (bottom). (d) Topography in bimodal AFM. (e) Phase shift image of the first mode in bimodal AFM. (f) Bimodal AFM phase image (second mode) of the same antibody. The image shows a Y-shaped object.
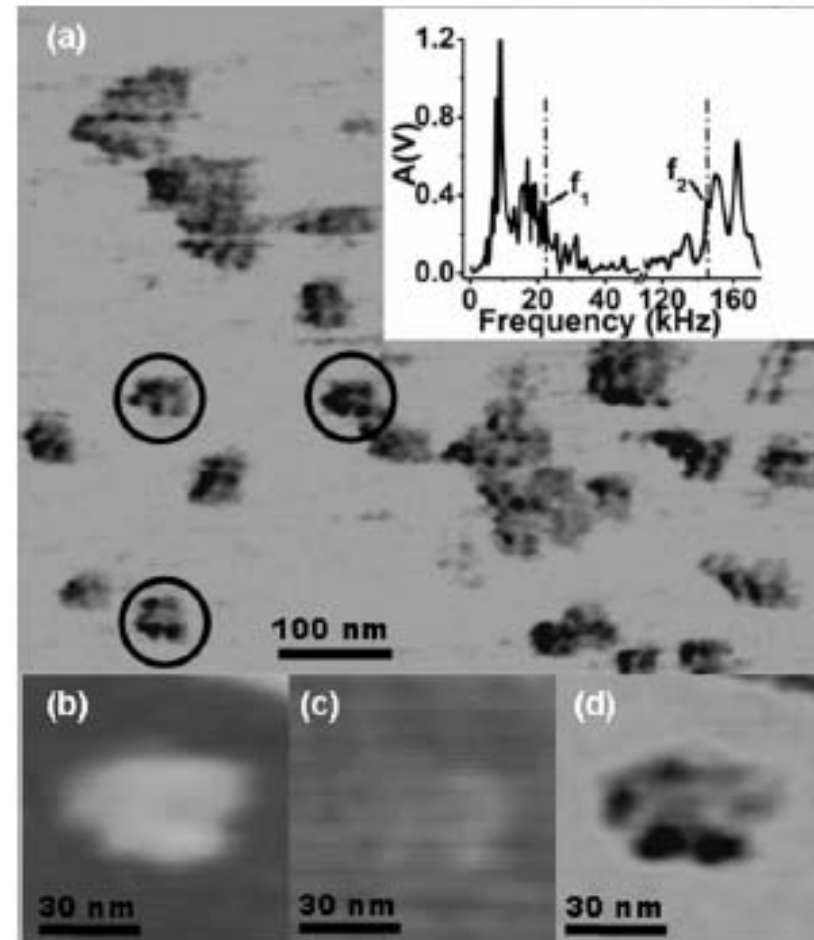
Figure 7. (a) Bimodal AFM phase images (second mode) of IgM antibodies in water. The objects that show a pentagonal shape are marked by circles. The inset shows the frequency spectrum of a commercial cantilever in water. The dashed lines indicate the frequencies of the first and second flexural modes of the cantilever. They were determined by measuring the thermal noise spectrum. (b) Topography of an isolated antibody. (c) First mode phase image and (d) bimodal AFM phase image (second mode) of the same antibody.

Martinez et al, Nanotechnology, 19, 2008

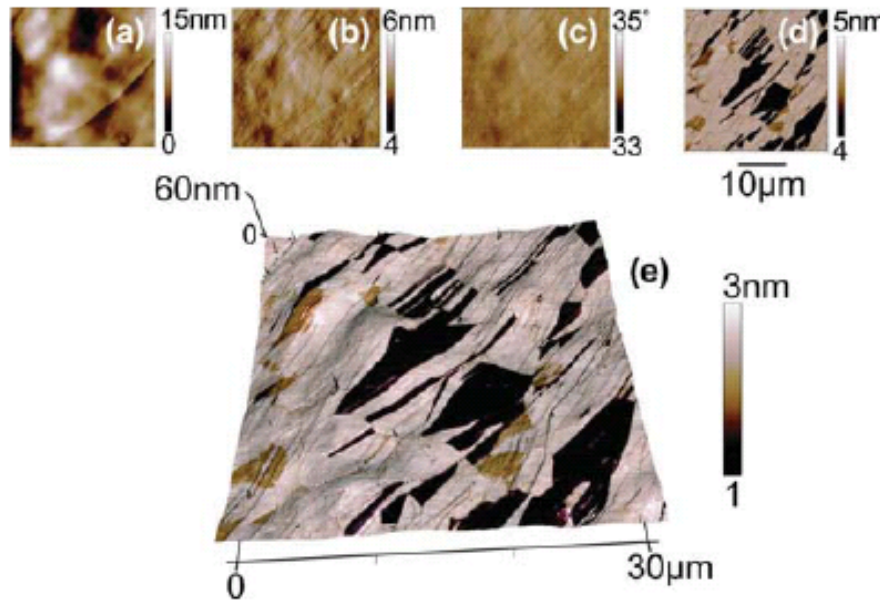# Multi-frequency AFM

- ## Bimodal or dual AC

FIG. 2. (Color online) HOPG graphite surface, 30 μm scan. The cantilever was driven at its fundamental (~69.5 kHz) and second eigenfrequency (~405 kHz). (a) shows the topography and (b) is the fundamental amplitude channel, used for the feedback error signal. The fundamental phase image (c) shows an average phase lag of ~34° indicating that the cantilever was in repulsive mode for the entire image. The second mode amplitude is shown in (d). The three dimensional rendered topography colored with the second mode amplitude is shown in (e). This method of display allows easy spatial correlation of the two channels.
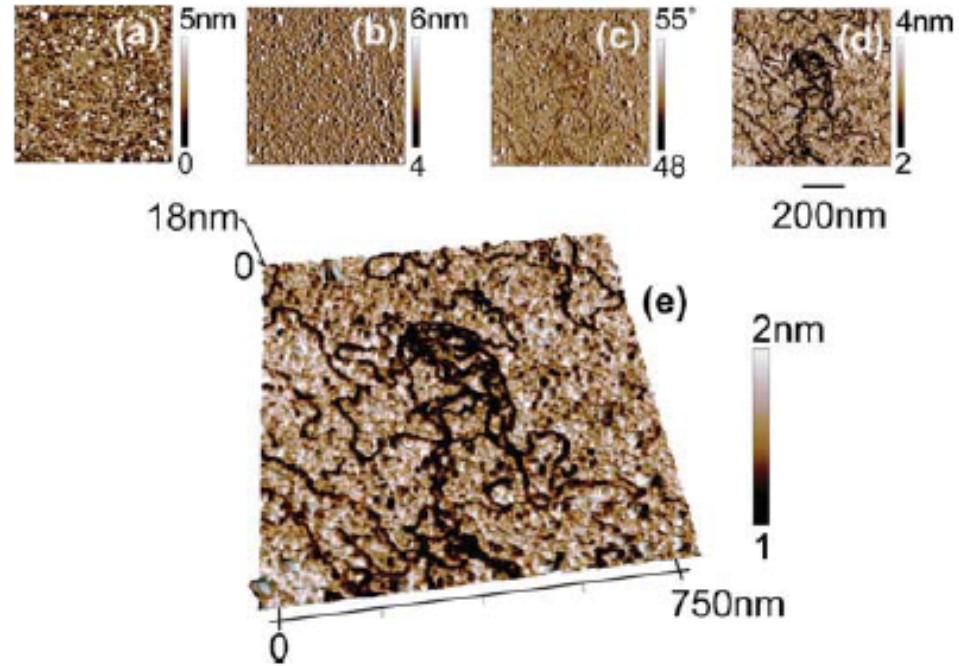
FIG. 3. (Color online) Dense mat of DNA imaged in buffer, 750 nm scan. The 60 μm Bio-Lever was driven at its fundamental resonance (~8.5 kHz) and at its second mode (~55 kHz). The topography (a), fundamental amplitude (b), and fundamental phase (c) all show very little differentiated contrast. The second mode amplitude (d) shows clear, high contrast images of what appear to be strands of DNA molecules. The second mode amplitude was painted onto the three dimensional rendered topography (e) to allow spatial correlation of the two data channels.
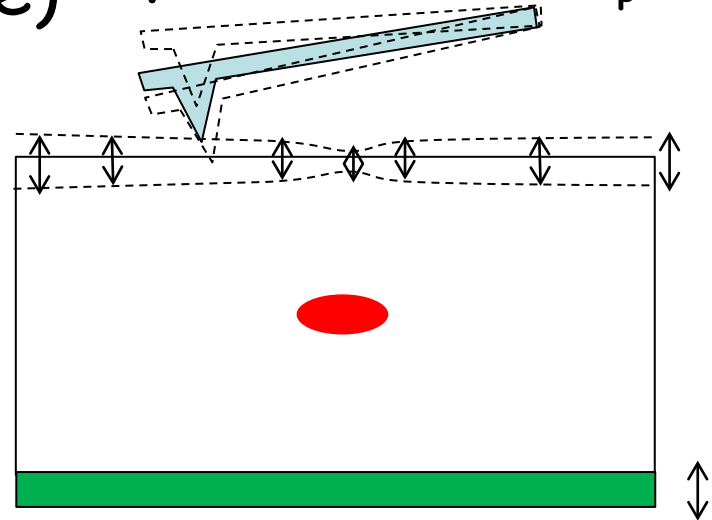
9

PURDUE
UNIVERSITY

Subsurface imaging using ultrasound

- Heterodyning principle for AFM first developed by Cuberes, Kolosov, Briggs (Oxford)

- Later used by Dravid et al (Northwestern), and Passian and Thundat (Oakridge)

HF probe excitation f_p (MHz

Sample surface vibration f_s
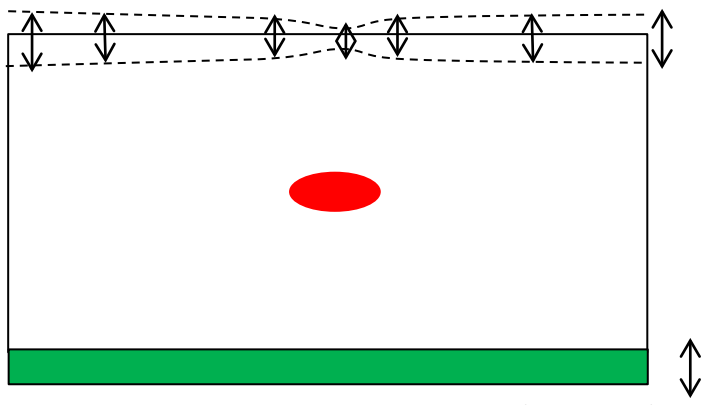
HF piezo excitation f_s (MHz)

HF piezo excitation f_s (MHz)

- Tip sample gap $d(t)=(.)\cos(f_s t)+ (.) \cos(f_p t)$

- Tip-sample force F_{ts} is a nonlinear function of d, so it contains frequency components including fs-fp

- Measure amplitude and phase of fs-fp signal

Nanoscale Imaging of Buried Structures via Scanning Near-Field Ultrasound Hol...
Gajendra S Shekhawat; Vinayak P Dravid
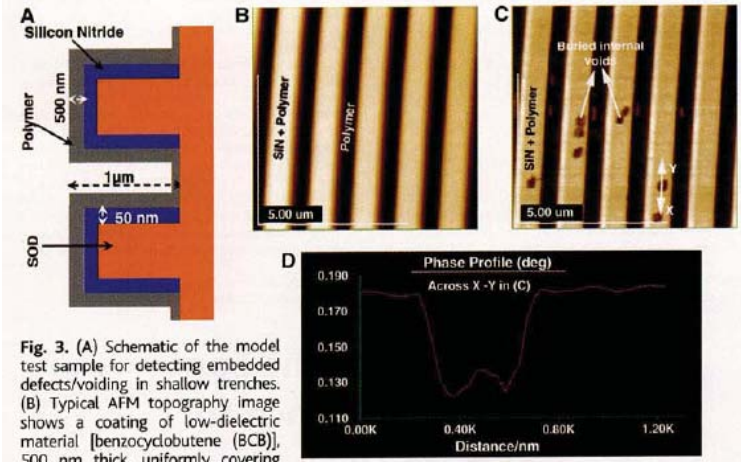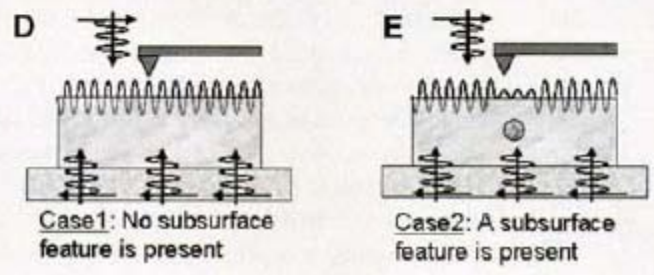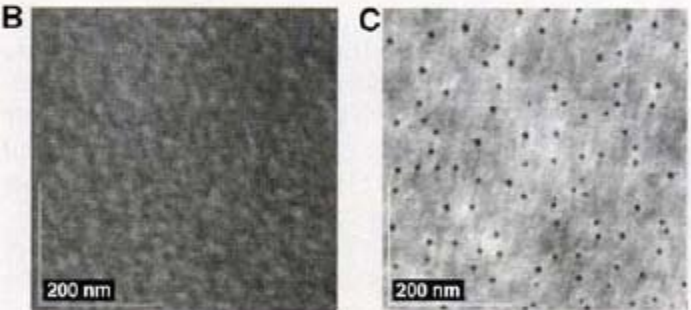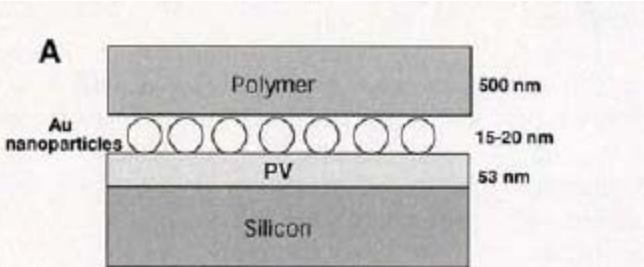*Science;* Oct 7, 2005; 310, 5745; Research Library Core
pg. 89

Fig. 3. (A) Schematic of the model test sample for detecting embedded defects/voiding in shallow trenches. (B) Typical AFM topography image shows a coating of low-dielectric material [benzocyclobutene (BCB)], 500 nm thick, uniformly covering the trenches. Trench width is ~400 nm and height is ~1 μm. (C) Phase image of SNFUH clearly reveals the surface elastic contrast and embedded voiding in polymer coating over nitride and hardening of it at the trench walls, a result of its curing. This is evident from the contrast at the trench walls. (D) The line profile across the void, marked across X-Y in (C). Remarkably high subsurface phase resolution is achieved
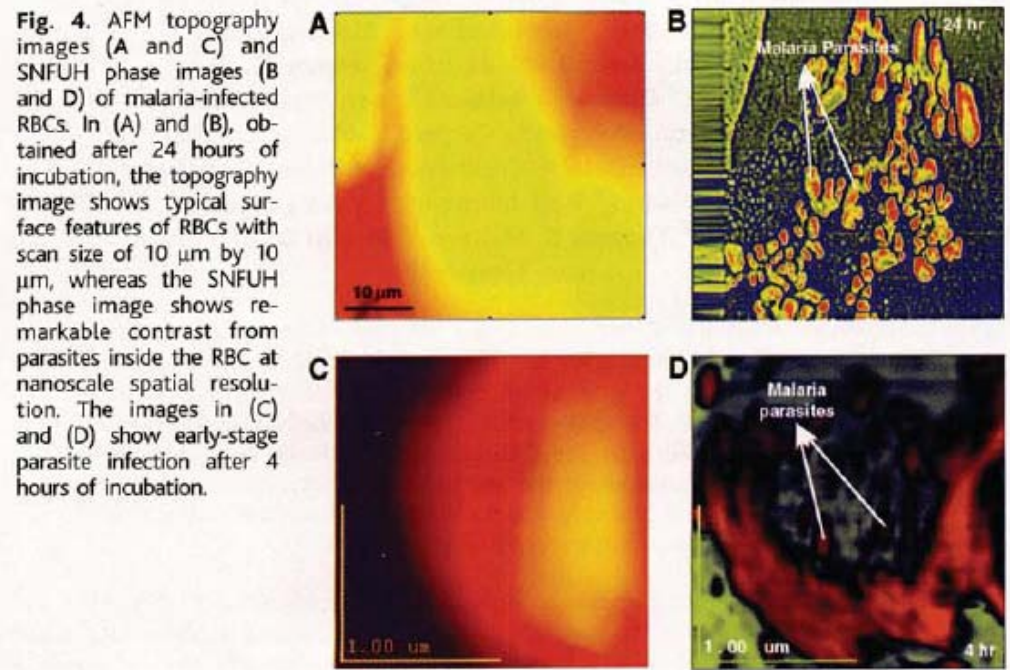
Fig. 4. AFM topography images (A and C) and SNFUH phase images (B and D) of malaria-infected RBCs. In (A) and (B), obtained after 24 hours of incubation, the topography image shows typical surface features of RBCs with scan size of 10 μm by 10 μm, whereas the SNFUH phase image shows remarkable contrast from parasites inside the RBC at nanoscale spatial resolution. The images in (C) and (D) show early-stage parasite infection after 4 hours of incubation.

LETTERS

Imaging nanoparticles in cells by nanomechanical holography

LAURENE TETARD[1,2], ALI PASSIAN[1,2]*, KATHERINE T. VENMAR[1], RACHEL M. LYNCH[1], BRYNN GAJENDRA SHEKHAWAT[3], VINAYAK P. DRAVID[3] AND THOMAS THUNDAT[1,2]

[1]Biosciences Division, Oak Ridge National Laboratory, Oak Ridge, Tennessee 37831, USA
[2]Department of Physics, University of Tennessee, Knoxville, Tennessee 37996-1200, USA
[3]Materials Science & Engineering department, Northwestern University, Evanston, Illinois 60208, USA
*e-mail: passianan@ornl.gov

Figure 3 Nanoparticles detected inside red blood cells. a–d, AFM topography (a,c) and SNFUH phase (b,d) images of erythrocytes obtained from the BAL fluid of an SWCNH-exposed mouse 24 h post-aspiration. e,f, Profiles taken along Γ'_1 and Γ'_2 across nanohorns buried in c and d, respectively, show that SNFUH can resolve nanoparticles that are inside the cells.
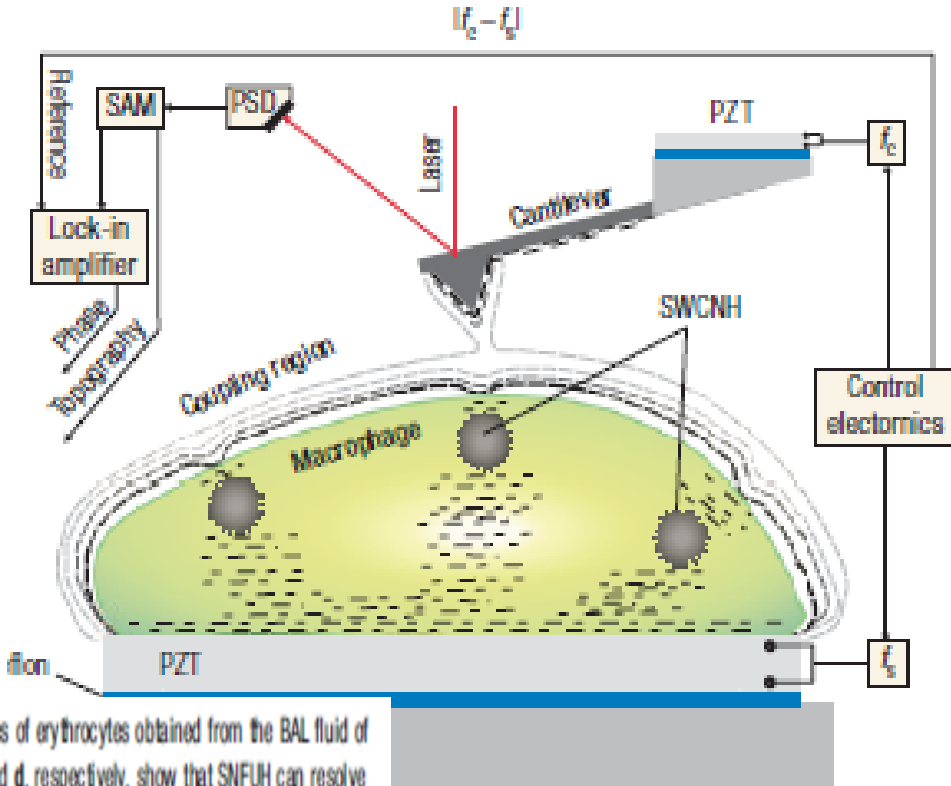
Figure 1 Intracellular imaging of aspirated nanoparticles using ultrasonic holography. The signal access module (SAM) provides the instantaneous location of the reflected laser beam as monitored by a position-sensitive detector (PSD). The dynamics of the cantilever is presented at the input of a lock-in amplifier. The local perturbation in the coupled oscillations of the ultrasonic-driven microcantilever–macrophage system is monitored with the lock-in using the difference frequency $f_c - f_s$ as reference. By mapping the strength of the coupling in a scanned area of the cell, a phase image emerges that contains information on the buried SWCNHs.

Challenges

- Not clear how mm wave length achieves high resolution
- **Not depth sensitive**
- Image formation not understood

PURDUE
UNIVERSITY